Solid State Sciences 32 (2014) 26–34

Contents lists available at ScienceDirect

Solid State Sciences

journal homepage: www.elsevier.com/locate/ssscie

Electrical transport properties of potassium germanide tungstates ($K_{10}Ge_{18}WO_4$): A theoretical study

Sikander Azam [a,*], A.H. Reshak [a,b]

[a] New Technologies – Research Center, University of West Bohemia, Univerzitni 8, Pilsen 306 14, Czech Republic
[b] Center of Excellence Geopolymer and Green Technology, School of Material Engineering, University Malaysia Perlis, 01007 Kangar, Perlis, Malaysia

ARTICLE INFO

Article history:
Received 29 December 2013
Received in revised form
27 February 2014
Accepted 22 March 2014
Available online 31 March 2014

Keywords:
Inorganic compounds
Semiconductors
Intermetallic compounds
Electronic structure
Optical properties
Thermal conductivity

ABSTRACT

The total and partial density of states, electronic charge density and optical properties of the monoclinic structure $K_{10}Ge_{18}WO_4$ compound have been investigated using a full relativistic version of the full-potential augmented plane-wave method based on the density functional theory, within local density approximation (LDA), generalized gradient approximation (GGA) and Engel-Vosko GGA (EVGGA). Density of states discloses the semiconductor nature of the calculated compound. There exists a strong hybridization between K-p and K-s, W-d and O-p, W-f and K-p. The analysis of the chemical bonding shows that the bonding possesses strong covalent nature. The dielectric optical properties were also calculated and discussed in detail. The electrical transport coefficients of the under observation compound have been investigated using the density functional theory calculation within EVGGA.

1. Introduction

The intermetallic compounds are the most important assembly of chemical compounds which can be made by two or more metals [1]. Now a days the intermetallic compounds are studied very broadly and ranges from magnetic mixtures and superconductors, refractory high-strength super alloys, to metallic crystal for feasible applications in fuels cells [2–4]. Moreover, the feasibility of functional intermetallic components has been validated by numerous disclosures of Zintl phases and polar intermetallics, which demonstrate complex combination of magnetic, thermal, electrical devices, structural, and transport properties [5–10]. From the last 3 decades the intermetallic compounds have been synthesized, whose structural and electronic devices characterizations have given fabulous information about their structure–property relationship [11–13].

Amongst the categories of an inorganic solids, the intermetallics are known as the most implicit with respect to their bonding properties [14,15]. Due to the information that some of the characteristics that mostly assessed the chemical bonding, i.e. the degrees of valence-electron move and localization, vary widely and approximately incessantly with the nature and composition of the elements involved [16,17].

Attributable to the important major electronegativity dissimilarities between the constituents, the combination of main assembly p-block elements (E) – which may be semimetals, metals, or small-gap semiconductors – with electropositive s-block active metals (alkali and alkaline-earth metals) recurrently escorts to so called “polar intermetallic” compounds that comprise polyanions of the post-transition elements. It is the significance of Zintl, [18–20] Klemm and other ones that some effortlessly applicable directions present for this subgroup of intermetallic mixtures. Mooser and Pearson [21–24] also Klemm and Busmann [25–28] discovered an association between the generalized 8-N direct and the possible anionic substructure in normal valence compounds (Zintl phases).

Unfortunately, previous work has paid much more attention to its crystal structure, structural topological [29]. The detailed theoretical studies in terms of electronic structure, electronic charge density, optical properties and electrical transport parameters for the aristocratic compound system are presently lacking. The very nature under these phenomena still desires farther investigation. The density function theory (DFT) calculation simulation method

* Corresponding author. Institute of Complex Systems, University of South Bohemia in CB, Nove Hrady 37333, Czech Republic. Tel.: +420 775928620.
E-mail addresses: sikander.physicst@gmail.com, sikandar_hu@yahoo.com (S. Azam).

http://dx.doi.org/10.1016/j.solidstatesciences.2014.03.014
1293-2558/

has been effectively directed in analyzing electronic structure, electronic charge density and optical properties of solid state materials [30–35], the Boltzmann transport form has also been effectively directed in electrical transport coefficients assessment of solid state components [36–38].

In the present work we have enquired the $K_{10}Ge_{18}WO_4$ system in regard to the electronic structure, electronic charge density and optical properties using the crystallographic data taken from the previous work of Siméon Ponou [29]. Also in the present work, we reported DFT investigations on the electric transport properties for $K_{10}Ge_{18}WO_4$ compound. The electric transport parameters (conductivity, Seebeck coefficient, power factor) for the compound scheme are obtained theoretically based on the DFT assessment outcomes and the rigid band approach for the first time to our knowledge. The TE properties are furthermore analyzed.

2. Methodology

The unit cell crystal structure of $K_{10}Ge_{18}WO_4$ compound has shown in Fig. 1. The investigated compound has monoclinic structure with space group number 14 ($P12_1/c1$). The lattice constants are $a = 13.908006324$ Å, $b = 15.90900754$ Å and $c = 17.383008012$ Å [29]. The experimental and the optimized atomic-positions are given in Table 1. The electronic structure and optical properties of $K_{10}Ge_{18}WO_4$ is studied using full potential linearized augmented plane wave as implemented in WIEN2k code [39]. The approach is based on density functional theory (DFT) [40,41]. The exchange correlation potential was calculated using local density approximation (LDA) of Ceperley–Alderas parameterized by Perdew–Zunger, generalized gradient approximation (GGA) of Perdew–Burke–Ernzerhof and EVGGA as modulated by Engel Vosko [42–44]. Kohn–Sham wave functions were expanded

Table 1
Experimental and optimized atomic positions.

Atoms	X (Exp.)[a]	X (Opt.)	Y (Exp.)[a]	Y (Opt.)	Z (Exp.)[a]	Z (Opt.)
W1	0.7537(1)	0.7517	0.0383(1)	0.0436	0.0047(1)	0.0085
O1	0.846(2)	0.8397	0.976(2)	0.9807	0.053(2)	0.0558
O2	0.664(2)	0.6611	0.974(2)	0.9784	0.962(2)	0.969
O3	0.700(2)	0.6978	0.099(2)	0.1088	0.075(1)	0.079
O4	0.806(2)	0.8053	0.093(1)	0.0969	0.930(1)	0.929
Ge1A	0.1906(2)	0.1983	0.3476(2)	0.3446	0.1604(3)	0.1649
Ge2A	0.0863(3)	0.0919	0.3371(2)	0.3329	0.0373(2)	0.0394
Ge3A	0.0447(3)	0.0470	0.4463(2)	0.4435	0.1515(3)	0.1573
Ge4A	0.0675(3)	0.0703	0.3182(2)	0.3144	0.2662(2)	0.2697
Ge5A	0.1156(3)	0.1213	0.2010(2)	0.1976	0.1552(2)	0.1513
Ge6A	0.9133(3)	0.9174	0.3684(3)	0.3719	0.0710(2)	0.0698
Ge7A	0.9019(3)	0.9013	0.3699(3)	0.3645	0.2179(2)	0.2203
Ge8A	0.0561(3)	0.0510	0.7111(3)	0.7030	0.2915(2)	0.2875
Ge9A	0.0285(3)	0.0300	0.7117(2)	0.7105	0.4374(2)	0.4366
Ge1B	0.4483(8)	0.4508	0.3219(5)	0.3278	0.3574(6)	0.3627
Ge2B	0.5915(6)	0.5944	0.2372(9)	0.2469	0.4363(7)	0.4279
Ge3B	0.4059(5)	0.4060	0.2022(5)	0.2027	0.4554(3)	0.4557
Ge4B	0.3628(4)	0.3655	0.2117(7)	0.2067	0.2974(6)	0.2861
Ge5B	0.5484(4)	0.5573	0.2471(4)	0.2493	0.2602(3)	0.2633
Ge6B	0.5369(6)	0.5410	0.0940(7)	0.0911	0.4478(6)	0.4542
Ge7B	0.3819(5)	0.3840	0.0753(6)	0.0695	0.3681(6)	0.3693
Ge8B	0.4999(5)	0.4981	0.0920(4)	0.0932	0.2618(3)	0.2529
Ge9B	0.6427(3)	0.6495	0.1395(4)	0.1298	0.3354(4)	0.3350
K1	0.1458(6)	0.1461	0.7515(5)	0.7477	0.1086(5)	0.1088
K2	0.1205(7)	0.1257	0.1039(5)	0.1009	0.3392(5)	0.3358
K3	0.2453(6)	0.2400	0.5032(5)	0.5006	0.0209(5)	0.0233
K4	0.2043(8)	0.2124	0.3201(5)	0.3231	0.4489(7)	0.4560
K5	0.7113(6)	0.7187	0.2557(6)	0.2648	0.1156(6)	0.1166
K6	0.0256(5)	0.0275	0.5151(6)	0.5174	0.6049(6)	0.6074
K7	0.6844(7)	0.6718	0.4474(8)	0.4479	0.3085(5)	0.3204
K8	0.2224(9)	0.2201	0.5276(7)	0.5283	0.2912(5)	0.2940
K9	0.4397(8)	0.4453	0.389(1)	0.3949	0.1447(7)	0.1481
K10	0.504(1)	0.4991	0.090(2)	0.1103	0.0668(9)	0.0595

[a] Ref. [29].

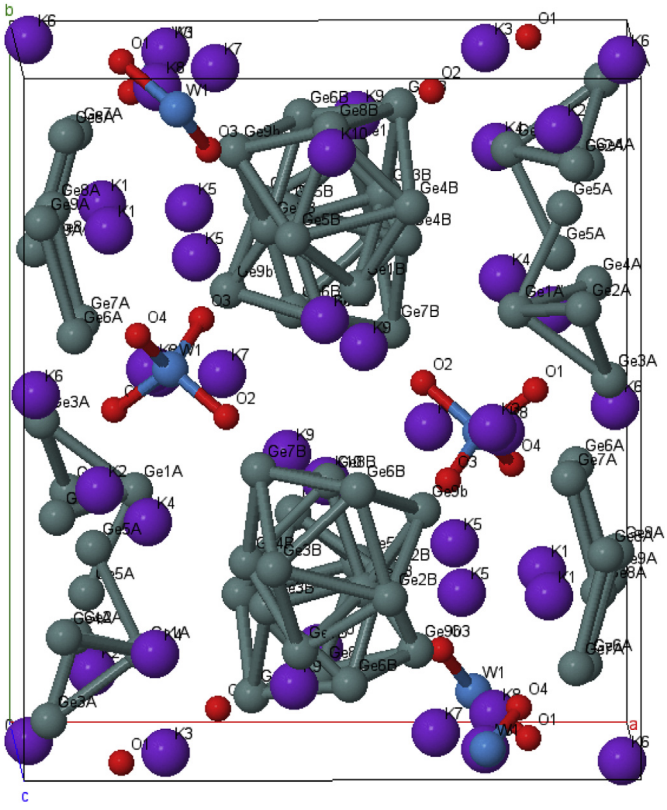

Fig. 1. Unit cell structure of $K_{10}Ge_{18}WO_4$.

in terms of spherical harmonic function in side the non-overlapping muffin- tin (MT) spheres and with Fourier series in the interstitial region. The ι-expansions of the wave functions were carried out up to $\iota_{max} = 10$ inside the muffin-tin spheres. The Fourier expansion for the charge density was up to $G_{max=}12$. The wave functions in the interstitial regions were expanded in the plane waves for the cut off $K_{MAx} \times R_{MT} = 7$ in order to achieve the convergence for energy eigen values. The valve for muffin-tin radii R_{MT} are chosen for $W = 1.63$ a.u, $O = 1.45$ a.u, Ge = 2.11 a.u, and $K = 2.3$ a.u.

In optical calculations, the dielectric function was calculated in the momentum representation, which requires matrix elements of the momentum p between occupied and unoccupied states. Thus, the components of the imaginary or the absorptive part of the dielectric function, $\varepsilon_2^{ij}(\omega)$ was calculated using the relation taken from Ref. [30];

$$\varepsilon_2^{ij}(\omega) = \frac{4\pi^2 e^2}{Vm^2\omega^2} \times \sum_{knn'\sigma} \langle kn\sigma|p_i|kn'\sigma\rangle\langle kn'\sigma|p_j|kn\sigma\rangle \times f_{kn}(1-f_{kn'})\sigma(E_{kn'} - E_{kn} - \hbar\omega)$$

where e is the electron charge and m is the and mass, ω is the frequency of the in coming electromagnetic radiation, V is the volume of the unit cell, $(p_x, p_y, p_z) = p$ is the momentum operator $\langle kn\sigma\rangle$ the crystal wave function, corresponding to eigenvalue E_{kn} with crystal momentum k and spin σ. Finally, f_{kn} is the Fermi distribution function ensuring that only transitions from occupied to unoccupied states are counted, and $\sigma(E_{kn'} - E_{kn} - \omega)$ is the condition for total energy conservation. The real part $\varepsilon_1(\omega)$ can be obtained from the imaginary part $\varepsilon_2(\omega)$ using the Kramer's Kronig dispersion relation [45].

$$\varepsilon_1(\omega) = 1 + \frac{2}{\pi} P \int_0^{\infty} \frac{\omega' \varepsilon_2(\omega')}{\omega' - \omega^2} d\omega'$$

The electric transport coefficients were premeditated in frame work of semi classical Boltzmann theory and the rigid band approach [37,38].

3. Results and discussion

3.1. Density of states

We have calculated the total and partial density of states using LDA, GGA and EV–GGA as illustrated in Fig. 2. From the density of states study we found that the band gap for LDA, GGA and EVGGA are 1.606, 1.746 and 2.01 eV. As there is no experimental data with which our calculated band gap should be compared but it is clear that the electronic band gap is always underestimated in DFT calculations [46,47]. The EV–GGA, gives an improved band splitting and other properties which depend on the accuracy of the exchange correlation potential. Therefore we will demonstrate only the results using EVGGA approximation. The density of states can be divided into several group structures separated by energy gaps. From PDOS we are able to identify the angular momentum origin of the various bands. The Fermi level is located at 0.0 eV.

Following Fig. 3, we should stress that there are four distinct structures separated from each others by gaps. The first structure encountered in the TDOS, if we start from lower energies, consists entirely of K–p and Ge-s/p states, these peaks are centred on around −11.5 to −11.1 eV. The next structure, laying between −9.25 and −8.5 eV for the investigated compound consist of K-p and Ge-s. The lower valence band i.e. from −6.9 to Fermi level consists of Ge-s/p/d, O-s/p, W-s/p/d/f with small contribution of K-s states. And also in this energy limit K-p and K-s, W-d and O-p along with W-f

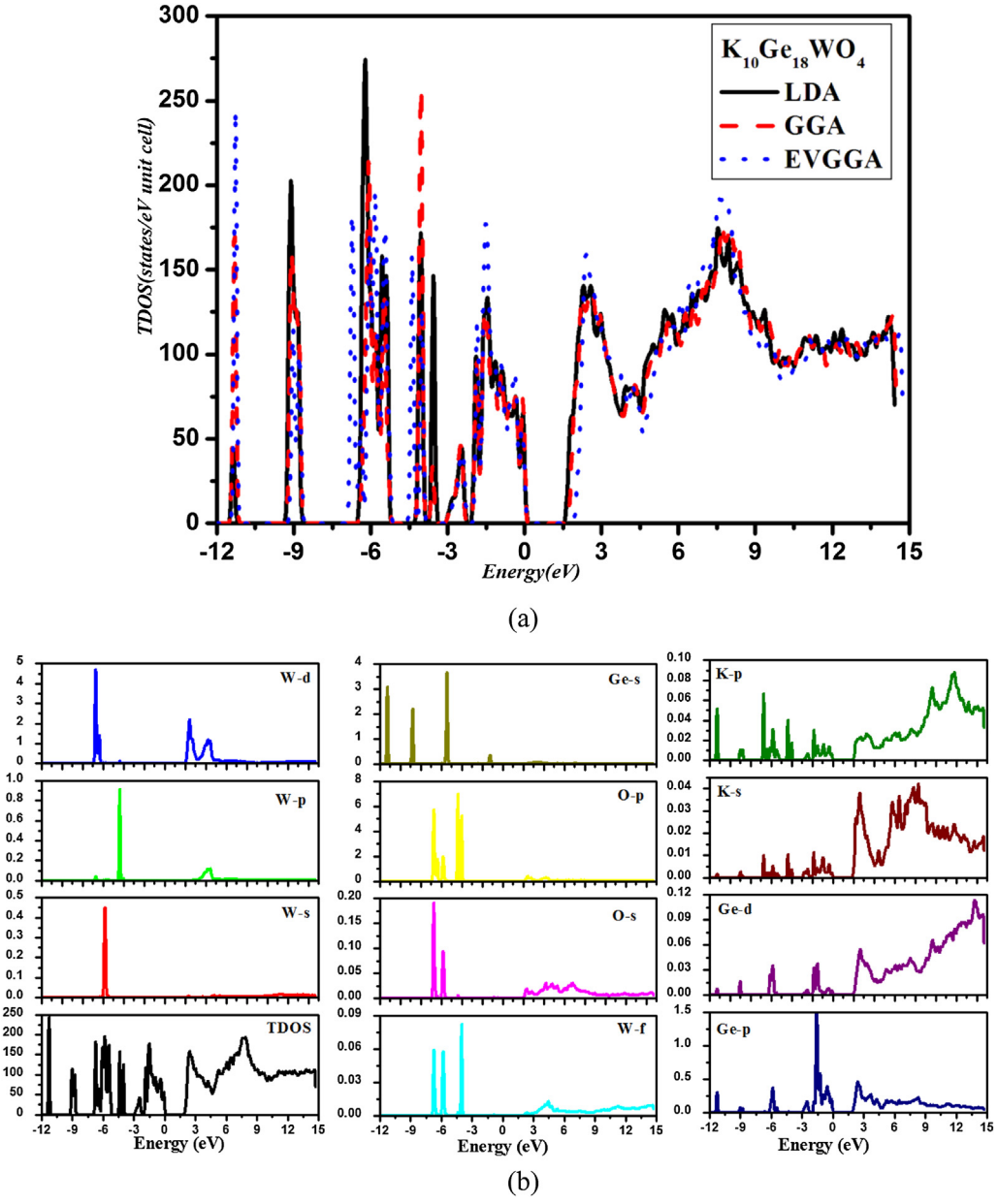

Fig. 2. Calculated total and partial densities of states (States/eV unit cell).

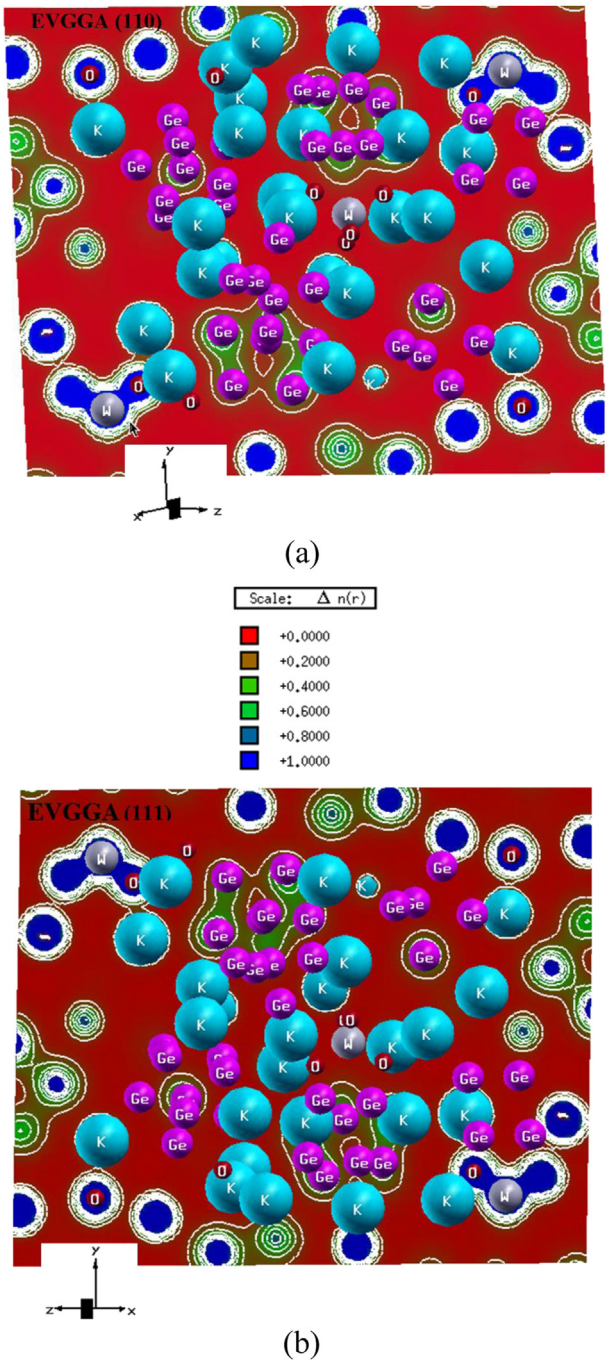

Fig. 3. Electronic charge density.

and K-p makes a strong hybridization. The conduction bands situated in the region between 1.95 eV and 16.0 eV consist of mainly K-s/p, W-d and Ge-p with small admixture of W-p/d states. The previous study also demonstrate that in most tungstates the bottom of the conduction band and the top of the valence band are dominated by W 5d states and O 2p states [46,47]. In the conduction band at the energy 2.0 eV–4.0 eV there is strong hybridization between K-s and K-p.

3.2. Electronic charge density

The recount of charge allocation in crystalline lattices has come a long way since the first quantum form of the atom. It was renowned from early days that a quantitative account of the chemical bonds in substances and crystals would need the assessment of the probability density of the electron cloud between atoms. The experimental possibility itself was advised soon after the breakthrough of X-ray diffraction. In the early days of 1915, Debye [48] claimed "that experimental cram of scattered emission, in exact from light atoms, should get more vigilance, since along this way it should be expected to work out the arrangement of electrons in the atoms". Assessment of charge densities in substances has been a preoccupation of theoretical pharmacists for sometime [49] and some charge density enquiries of crystalline solids by both trial and idea have been described in the literature [50–58].

The electronic charge density allocation in a molecule or a crystal may be got by Hartree–Fock (HF) computed results [59]. It involves assessment of anti symmetrized many-electron signal function and minimizing the energy with esteem to the coefficients of the one-electron signal function. When the energy is minimized, the wave function is said to have accomplished self consistency (SCF). Slater type atomic orbital were used in the ancient times which impersonated allotment of adversity in analytically integrating the polynomial purposes. Use of Gaussian purposes in the radial part of the wave function has made HF procedure more appropriate.

In the current manuscript we also calculated the electronic charge density in order to understand the behaviour of the atoms in the compound by using the FPLAPW method. To further study the interaction among W, K, Ge and O atoms, the contour maps of electronic charge densities for EVGGA in the 2D (110) plane is shown in the Fig. 3(a). We also plotted the electronic charge density for EVGGA in (111) plane as shown in Fig. 3(b), in order to study the anisotropic behaviour of the electronic charge density in changing from one plane to the other in the crystal. The plot shows partial ionic and covalent bonding between K and Ge, which acting on the Pauling electro-negativity difference of Ge (2.55) and K (3.44) atoms. The calculated electron density shows that charge density lines are spherical in some areas of the plane structure which shows sign of ionic bond between O atoms and in some areas of structures K and Ge atoms shared electron that shows the strong covalent interaction between Ge–Ge, O–W and O–k. Due to the electronegativity differences between K, Ge, and H atoms, thus most the charges are transferred to O site.

The electronic charge density (ECD) contour shows anisotropy of the investigated compound. As we have plotted the ECD in (110) and in (111) plane, so as it is clear from the (110) that between Ge and O is the weak covalent bonding while in the (110) plane both the two atoms (Ge and K) attract each other but only the charge density contour around the K is disturbed. The charge density round the Ge–Ge covalent bond in (110) is less than the (111) plane. And also Ge atoms shows much greater charge density (110) than the Ge atom in the (111) plane. We also have calculated the bond length and bond angle which are in good agreement with the previous calculated work [29] as shown in Tables 2 and 3. Also our calculated Ge–Ge intracluster distances are similar to those in e.g. Cs_4Ge_9 (2.522(8) Å – 3.008(11) Å) [60]. The W–O distances are similar to those of most tungstates [61]. This happen because WO_4 tetrahedra are very rigid unit that are not influenced by the crystal field created by other atoms Table 3.

3.3. Linear optical response

To understand the physical origins of optical properties, the relation stuck between electronic structure and molecular orbital bonding should be elucidated due to the origins of absorption peaks

Table 2
Experimental and optimized bond length.

Atomic pair	Distance (Å) Exp.[a]	Distance (Å) our work	Atomic pair	Distance (Å) Exp.[a]	Distance (Å) our work
O1–K4	2.58	2.618	K4–Ge3B	3.38	3.304
O1–K6	2.65	2.763	K4–Ge2A	3.36	3.326
O1–K8	2.98	2.841	K4–Ge1B	3.75	3.691
O1–K6	3.34	3.436	K4–Ge4A	3.70	3.796
O2–K10	2.60	2.685	K4–Ge5A	3.81	3.639
O2–K7	2.97	2.843	K4–Ge9A	3.83	3.891
O2–K10	3.42	3.456	K4–Ge4B	3.84	4.084
O2–K4	3.42	3.299	K5–Ge6A	3.42	3.348
O3–K5	2.59	2.583	K5–Ge5B	3.39	3.674
O3–K10	2.74	2.785	K5–Ge2B	3.53	3.857
O3–K8	2.81	2.791	K5–Ge7A	3.67	3.495
O4–K1	2.66	2.647	K5–Ge8A	3.68	3.740
O4–K6	2.72	2.742	K5–Ge9A	3.80	3.717
O4–K7	2.78	2.750	K6–Ge5A	3.76	3.741
O4–Ge7A	3.72	3.024	K6–Ge7A	3.72	3.669
K1–Ge9A	3.44	3.466	K6–Ge9A	3.76	3.793
K1–Ge8A	3.48	3.451	K6–Ge4A	3.71	3.684
K1–Ge9B	3.57	3.541	K7–Ge7A	3.63	3.869
K1–Ge7A	3.62	3.564	K7–Ge5B	3.80	3.674
K1–Ge2B	3.75	3.664	K7–Ge7B	3.80	3.903
K1–Ge6A	3.75	3.749	K7–Ge8B	3.66	3.544
K1–Ge4A	3.83	3.827	K7–Ge1B	3.94	3.694
K2–Ge3A	3.41	3.472	K8–Ge9B	3.40	3.306
K2–Ge5A	3.55	3.559	K8–Ge3A	3.70	3.642
K2–Ge2A	3.60	3.721	K8–Ge1A	3.68	3.703
K2–Ge7B	3.70	3.673	K8–Ge8A	3.73	3.643
K2–Ge4A	3.71	3.668	K9–Ge5B	3.38	3.435
K2–Ge4B	3.85	3.835	K9–Ge1A	3.54	3.539
K2–Ge8A	3.76	3.646	K9–Ge3B	3.62	3.728
K2–Ge7A	3.86	3.903	K9–Ge6B	3.65	3.631
K3–Ge6A	3.40	3.395	K9–Ge8B	3.72	3.679
K3–Ge6B	3.40	3.390	K9–Ge1B	3.85	3.881
K3–Ge2A	3.46	3.383	K9–Ge7B	3.88	3.666
K3–Ge1A	3.55	3.535	K9–Ge6B	3.69	3.631
K3–Ge7B	3.50	3.525	K10–Ge8B	3.39	3.371
K3–Ge9B	3.66	3.556	K10–K10	3.70	4.076
K3–Ge3A	3.71	3.668	K10–Ge2B	3.76	3.485
Ge1A—Ge5A	2.556	2.582	Ge1B–Ge4B	2.36	2.624
Ge1 A–Ge4 A	2.556	2.599	Ge1B–Ge5B	2.49	2.596
Ge1 A–Ge3 A	2.570	2.630	Ge1B–Ge2B	2.77	2.632
Ge1 A–Ge2 A	2.589	2.634	Ge1B–Ge3B	2.62	2.638
Ge2 A–Ge6 A	2.526	2.560	Ge2B–Ge9B	2.45	2.582
Ge2 A–Ge9 A	2.593	2.615	Ge2B–Ge6B	2.41	2.628
Ge2 A–Ge3 A	2.700	2.774	Ge2B–Ge3B	2.66	2.756
Ge2 A–Ge5 A	3.009	2.929	Ge2B–Ge5B	3.12	2.908
Ge3 A–Ge6 A	2.611	2.620	Ge3B–Ge6B	2.51	2.585
Ge3 A–Ge7 A	2.599	2.624	Ge3B–Ge7B	2.55	2.615
Ge3 A–Ge4 A	2.868	2.854	Ge3B–Ge4B	2.81	3.001
Ge4 A–Ge7 A	2.585	2.627	Ge4B–Ge7B	2.51	2.631
Ge4 A–Ge8 A	2.618	2.657	Ge4B–Ge5B	2.72	2.781
Ge4 A–Ge5 A	2.765	2.862	Ge4B–Ge8B	2.77	2.645
Ge5 A–Ge9 A	2.576	2.610	Ge5B–Ge9B	2.52	2.610
Ge5 A–Ge8 A	2.567	2.624	Ge5B–Ge8B	2.56	2.623
Ge6 A–Ge7 A	2.557	2.629	Ge6B–Ge9B	2.55	2.636
Ge6 A–Ge9 A	2.625	2.672	Ge6B–Ge7B	2.58	2.658
Ge7 A–Ge8 A	2.598	2.657	Ge7B–Ge8B	2.49	2.600
Ge8 A–Ge9 A	2.566	2.610	Ge8B–Ge9B	2.46	2.610
Ge6 A–Ge8 A	3.485	3.682	Ge6B–Ge8B	3.28	3.551
Ge7 A–Ge9 A	3.818	3.790	Ge7B–Ge9B	3.81	3.862
W1–O4	1.72	1.776	O1–O2	2.99	2.905
W1–O3	1.72	1.774	O1–O3	2.84	2.865
W1–O2	1.78	1.770	O1–O4	2.88	2.908
W1–O1	1.83	1.782	O2–O3	2.84	2.867

[a] Ref [29].

Table 3
Experimental and optimized bond angles.

Oi − W − Oj angles	Experimental[a]	Our work
O1–W–O2	111.9	109.73
O1–W–O3	106.4	107.37
O1–W–O4	108.8	109.66
O2–W–O3	108.5	108.01
O2–W–O4	106.0	106.32
O3–W–O4	115.4	115.66

[a] Ref [29].

of optical properties from the electrons transition. In solid the optical properties are account by dielectric tensor. The investigated crystal has monoclinic symmetry, which has five nonzero components of the second-order dielectric tensor. In regardless of this only $\varepsilon^{xx}(\omega)$, $\varepsilon^{yy}(\omega)$ and $\varepsilon^{zz}(\omega)$ are major components so we concentrate on these three major frequency-dependent dielectric function components.

Based on the electronic structure, the dielectric functions of $K_{10}Ge_{18}WO_4$ have been calculated. The $\varepsilon_2(\omega)$ and $\varepsilon_1(\omega)$ spectra as a function of the photon energy are shown in Fig. 4. The imaginary part $\varepsilon_2(\omega)$ of the dielectric function is directly connected with the energy band structure. The threshold peak of the imaginary part appears at about 0.5 eV that is related to the transition from the top of valence band to the bottom of conduction band. The first peak 'E1' at about 2.2 eV corresponds to the transition from Ge-p in VB to O-s in CB, and the second peaks are ascribed to the transition of inner electron excitation from Ge-d in VB to either O-s or W-p in CB. The results for the dispersive part of the dielectric function $\varepsilon_1(\omega)$ are shown in Fig. 4(b). For the real part $\varepsilon_1(\omega)$, it presents the main peak at 2.2 eV. And it reduces to a minimum at energy above 4.0 eV. At high frequencies the zero crossing of $\varepsilon_1(\omega)$ which corresponds to the location of the screened plasma frequency is located at 3.9 eV for the three components. The region below the zero line shows the reflectivity i.e. this region shows the metallic behaviour of the material and the above region from the line shows the transmission of the light. From the real part it is clear that the material shows metallic behaviour at higher energies.

Fig. 4(c)–(e) shows the calculated results on the refractive index, reflectivity and energy-loss spectrum respectively. The calculated refractive index is demonstrated in Fig. 4(e). The refractive index is a very imperative physical parameter associated to the microscopic atomic interactions. From theoretical outlook point, there are basically two distinct approaches of examining this subject, the refractive index $n(\omega)$ will be associated to the density and the local polarizability of these entities [62]. On the other hand, considering the crystalline structure comprised by a delocalised picture, $n(\omega)$ will be nearly related to the power band structure of the material, quantum mechanical analysis obligations is perplexing and the got outcomes are very specific. Consequently, numerous endeavours have been made in order to relate the refractive catalogue and the energy gap Eg through simple connections [63–68].

The static refractive index $n(0)$ is found to have the values 2.725, 2.759 and 2.714 for $n^{xx}(0)$,$n^{yy}(0)$ and $n^{zz}(0)$ respectively. It increases with energy in the transparency region reaching a peak in the ultraviolet at about 2.2 eV. It then decreases to a minimum level at 3.2 eV. The origin of the structures in the imaginary part of the dielectric function also explains the structures in the refractive index.

The electron energy loss function $L(\omega)$ is an important factor describing the energy loss of a fast electron traversing in a material, and its sharp peak is usually associated with the plasma energy as shown in Fig. 4(c). The prominent peaks in $L(\omega)$ spectra represent the characteristic associated with the plasma resonance (a collective oscillation of the valence electrons) and the corresponding frequency is the so-called plasma frequency ω_p. The peaks of $L(\omega)$ correspond to the trailing edges in the reflection spectra, for instance, the prominent peaks of $L(\omega)$ (Fig. 4(c)) are situated at energies corresponding the abrupt reductions of $R(\omega)$ (Fig. 4(d)).

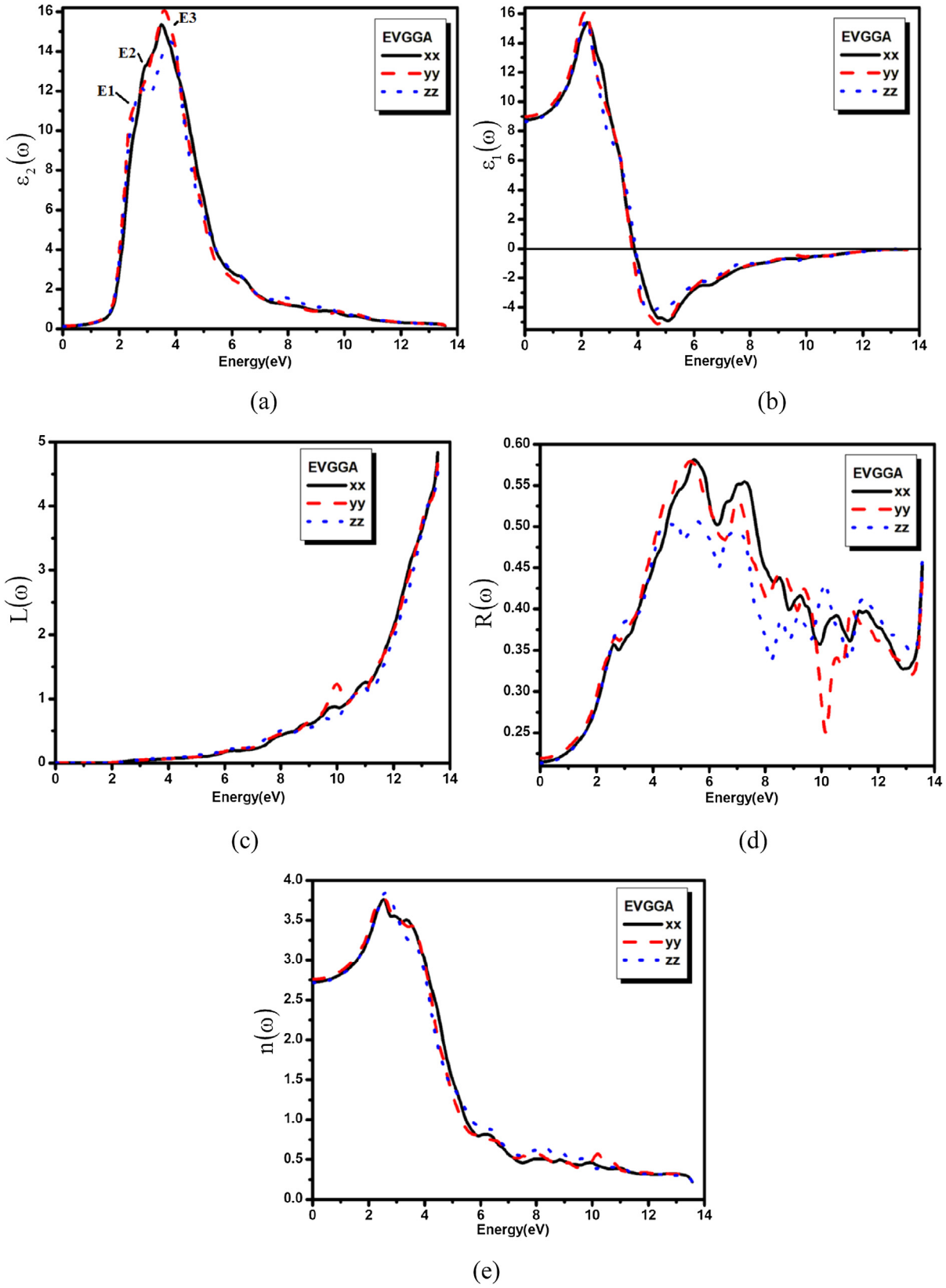

Fig. 4. Calculated imaginary $\varepsilon_2(\omega)$ and real part $\varepsilon_1(\omega)$ of dielectric tensor and other related optical properties.

3.4. Electrical transport properties

The growing energy crisis requires human beings to develop new energy solutions now a day. Thermoelectric (TE) materials which can convert heat energy in to electrical energy directly have attracted more and more attention during the last two decades [69,70]. They afford a promising way collecting waste heat energy renewably with in industrial production fields. Good TE materials should have high Seebeck coefficient α, low electrical resistivity ρ and total thermal conductivity κ at the same time. The traditionally typical TE material systems are heavily doped alloy semiconductors with low thermal conductivity κ simultaneously providing a balance between a large Seebeck coefficient α and a low electrical resistivity ρ [71].

The thermoelectric properties of the samples as a function of the temperature in the range from 300 K to 800 K are presented in Fig. 5. For the conductivity coefficient calculation, the relaxation time term τ should be treated as a constant parameter. Fig. 5(a) presents the calculated temperature dependent electrical conductivities for monoclinic $K_{10}Ge_{18}WO_4$ compound as a function of relaxation time $\sigma(\tau)$ within the temperature interval from 300 K to 800 K. The $\sigma(\tau)$ value increase rapidly along with increasing

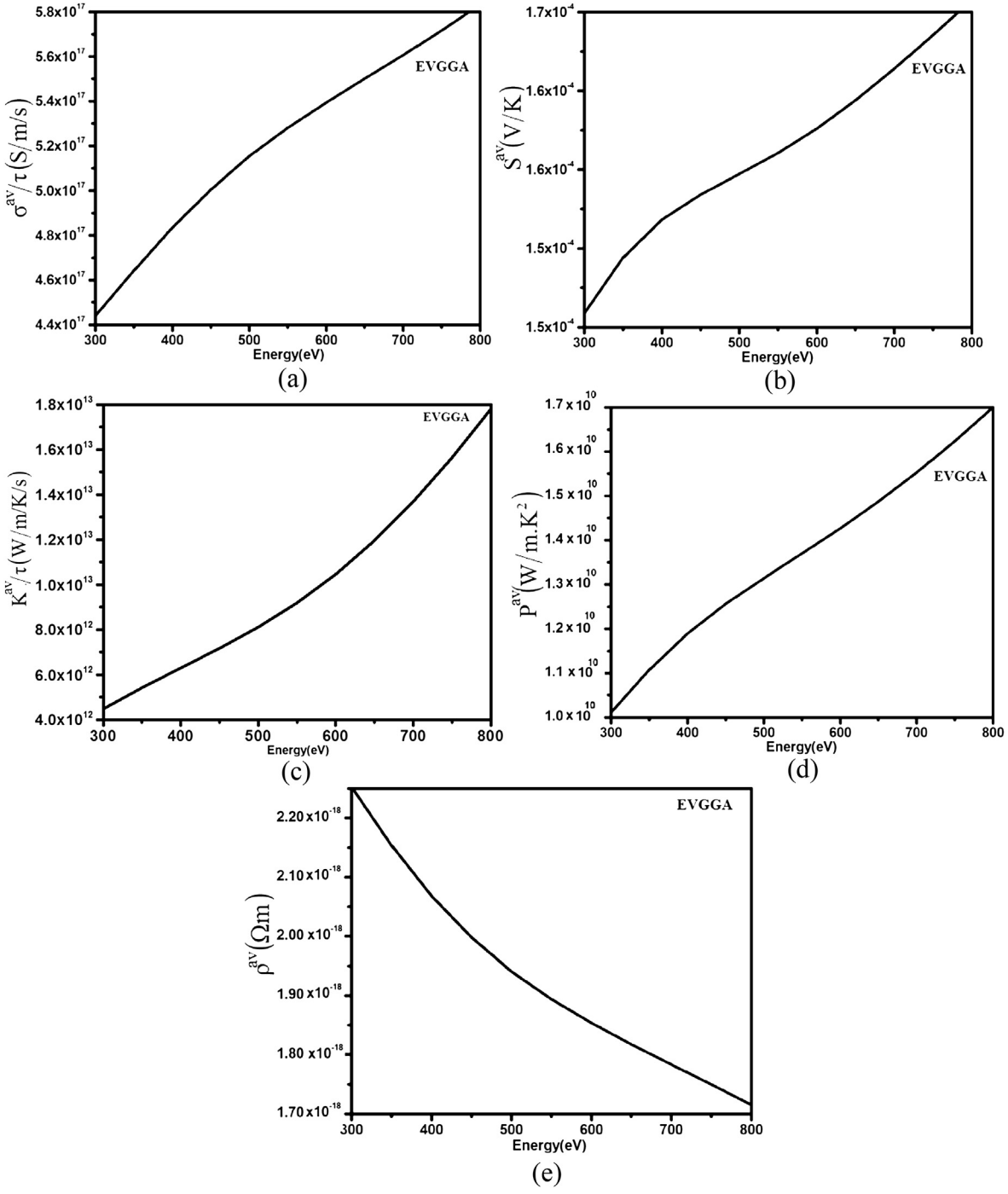

Fig. 5. Calculated thermoelectric properties i.e. Seebeck coefficients, electrical conductivity, thermal conductivity and power factor.

temperature, confirming the semiconductor like transportation and temperature sensitive conduction; this is in good agreement with its band.

Fig. 5(b) demonstrates that the introduction of $K_{10}Ge_{18}WO_4$ generates an increased in average Seebeck coefficient (S). It is considered that the Seebeck coefficient and the conductivity for a specific solid state material are antagonistically correlated with carrier density. Furthermore, in consideration of the conductivity dependence as a function of temperature, the electrical performance should be enhanced with elevating the temperature.

The magnitude of the thermopower (S) is temperature dependent, and rapidly increasing toward high peaks as the temperature increases. The positive Seebeck coefficient (S) of all the samples indicates p-type electrical transport behaviour. This phenomenon can be explained by the equation

$$S = \pm\frac{k_B}{e}\left[2 + \ln\frac{2(2\pi m^* k_B T)^{\frac{3}{2}}}{h^3 n}\right]$$

in which m^* is the density of states effective mass and n is the charge carrier concentration. Holes being the majority carriers are consistent with their higher mobility and greater effective mass than the electrons carriers. Here in, according to the equation, the S is increased. The increased in thermo-power is due to the thermal de-excitation of electrons across the band gap. As a result of the increased S, the power factors were also increased as shown in Fig. 5(d).

The Seebeck coefficient is not the only number that determines the usefulness of a material in a thermoelectric generator or a thermoelectric cooler. Under a given temperature coolness, the ability of a material to produce useful electrical power is quantified by its power factor.

$$PF = S^2\sigma$$

where S is Seebeck coefficient and σ is the electrical conductivity. Material with high power factor is able to generate more energy in a space-constrained application, but they are not necessarily efficient. Fig. 5(d) shows the temperature dependent power factor which increases monotonically within the whole temperature range. The value increases rapidly above 300 K and followed with an almost linear increase with increased in temperature. The large power factor was obtained in the cases of low electrical resistivity. Fig. 5(d) presents the calculated temperature dependent power factor P as a function of relaxation time within the temperature interval from 300 K to 800 K. The P values increase rapidly along with increasing temperature, confirming the temperature sensitive electrical performance.

The Fig. 5(a) shows the calculated electrical conductivity. The results follow the trend that the electrical conductivity increases with increasing temperature and it exhibits semiconductor-like behaviour. To obtain σ and κ_e, one needs to know the relaxation time τ. From the σ/τ values, we obtained a set of the temperature dependent relaxation times s as shown in Fig. 5(a). The relaxation time shows an increasing trend with increasing the temperature due to the increase in the mobility at the higher temperature. As we see that by increasing the temperature the conductivity of the investigated material increases. The temperature dependence of the thermal conductivity k is shown in Fig. 5(c). The electronic thermal conductivity was estimated with the Wiedeman-Franz law $\kappa_e = L_0 T\sigma$ where L_0, σ and T are Lorentz number, electrical conductivity and temperature respectively. The thermal conductivities increase rapidly with increasing temperature, which indicates that phonon conductivity dominates. Fig. 5(e) shows the temperature dependent electrical resistivity of the investigated compound. Transport behaviour changes in the whole selected range temperature. The resistivity drops rapidly with increasing temperature below 300 K indicating a semiconducting behaviour.

4. Conclusion

Our present paper accounts a systematic study on the density of states, electronic charge density and optical properties of $K_{10}Ge_{18}WO_4$ compound utilizing the FP-LAPW method within LDA, GGA and EVGGA. For density of states, electronic charge density and optical properties the assessment provides a very good description of the calculated properties of the investigated compound. The charge density has been offered and it displays the covalent character of Ge–Ge, O – W and O – k bonds. We have furthermore offered the dielectric tensor components of the $K_{10}Ge_{18}WO_4$. Our outcomes for the real and the invented components of the dielectric functions are used to duplicate optical constants, such as the absorption, refractive index, extinction coefficient, electron energy-loss and reflectivity. In addition we have granted assignments for the most significant transitions taking into account density of states calculations. We also have calculated the electrical transport coefficients of $K_{10}Ge_{18}WO_4$ have been studied. The Seebeck coefficient together with the conductivity and the power factor both as a function of relaxation time are calculated systematically. The TE properties are also analyzed. The calculated conductivity and Seebeck coefficient results confirm the semiconductor transport behaviour. The calculated power factor as a function of relaxation time increases rapidly with increasing temperature. The present calculation results should be helpful in understanding TE behaviours of other Zintl phase compound.

Acknowledegment

The result was developed within the CENTEM project, reg. no. CZ.1.05/2.1.00/03.0088, co-funded by the ERDF as part of the Ministry of Education, Youth and Sports OP RDI programme.

References

[1] P. Villars, L.D. Calvert, Pearsons Handbook of Crystallographic Data for Intermetallic Compounds, second ed., ASM International, Materials Park, OH, 1991. Desk Edition, 1997.
[2] C.T. Sims, N.S. Stoloff, W.C. Hagel, Superalloys II, Wiley, New York, 1987.
[3] J.F. Herbst, in: G.J. Long, F. Grandjean (Eds.), Supermagnets, 1991.
[4] H. Hillman, in: S. Foner, B. Schwartz (Eds.), Superconductor Materials Science-Metallurgy, Fabrication and Applications, 1981, p. 275. New York.
[5] R.B. Schwartz, in: J.H. Westbrook, R.L. Fleischer (Eds.), Intermetallic Compouds, vol. 3, Wiley, New York, 2002, p. 681.
[6] J. Nagamatsu, N. Nakagawa, T. Muranaka, Y. Zenitani, J. Akimitsu, Nature 410 (2001) 6824.
[7] J.Y. Chan, S.M. Kauzlarich, P. Klavins, R.N. Shelton, D.J. Webb, Chem. Mater. 9 (1997) 3132.
[8] A.M. Campbell, Science 292 (2001) 65.
[9] D.-Y. Chung, T. Hogan, P. Brazis, M. Rocci-Lane, C. Kannerwurf, M. Bastea, C. Uher, M. Kanatzidis, Science 287 (2000) 1024.
[10] H. Kawaji, H. Horie, S. Yamanaka, M. Ishikawa, Phys. Rev. Lett. 74 (1995) 1427.
[11] W.B. Pearson, The Crystal Chemistry and Physics of Metals and Alloys, Wiley-Interscience, New York, 1972.
[12] P. Villars, in: J.H. Westbrook, R.L. Fleischer (Eds.), Intermetallic Compounds Principles and Practice, 1, John Wiley & Sons, Chichester, U.K, 1994, pp. 227–275.
[13] W. Hume-Rothery, R.E. Smallman, C.W. Haworth, in: The Structure of Metal and Alloys, fifth ed., Anthony Rowe Ltd, Chippenham, Wilts, 1969.
[14] L. Pauling, in: A. Zewail (Ed.), The Chemical Bond – Structure and Dynamics, Boston Academic Press, Inc., 1992, p. 99.
[15] R. Nesper, Prog. Solid State Chem. 20 (1990) 1.
[16] G.J. Miller, in: S.M. Kauzlarich (Ed.), Chemistry, Structure and Bonding of Zintl Phases and Ions, VCH Publishers, New York, 1996.
[17] T.F. Fässler, S.Z. Hoffmann, Kristallogr. 214 (1999) 722.
[18] E. Zintl, G. Brauer, Z. Phys. Chem. B 20 (1933) 245–271.
[19] E. Zintl, P. Woltersdorf, Z. Electrochem. 41 (1935) 876–900.

[20] E. Zintl, Angew. Chem. 52 (1939) 1.
[21] E. Mooser, W.B. Pearson, Phys. Rev. 101 (1956) 1608.
[22] E. Mooser, W.B. Pearson, Acta Crystallogr. 12 (1959) 1015.
[23] E. Mooser, W.B. Pearson, in: Gibson, Kröger, Burgess (Eds.), Progress in Semiconductors, vol. 5, Wiley & Sons Inc., New York, 1960, 103.
[24] W.B. Pearson, Acta Crystallogr. 17 (1964) 1.
[25] W. Klemm, Proc. Chem. Soc. London (1958) 329–341.
[26] E.Z. Busmann, Anorg. Allg. Chem. 313 (1961) 90, Chap. 1 10 Introduction TU München 2006 Dissertation Ponou.
[27] W. Klemm, in: F. Sauter (Ed.), Festkoerperprobleme, 3, Vieweg, Braunschweig, Germany, 1963, pp. 233–251.
[28] W. Klemm, E. Busmann, Z. Anorg. Allg. Chem. 319 (1963) 297.
[29] Siméon Ponou, PhD thesis, 2006.
[30] Sikander Azam, A.H. Reshak, Int. J. Electrochem. Sci. 8 (2013) 10359–10375.
[31] A.H. Reshak, Sikander Azam, Int. J. Electrochem. Sci. 8 (2013) 10396–10423.
[32] A.H. Reshak, S. Azam, J. Magn. Magn. Mater. 345 (2013) 294–303.
[33] A.H. Reshak, S. Azam, J. Magn. Magn. Mater. 342 (2013) 80–86.
[34] Saleem Ayaz Khan, A.H. Reshak, Int. J. Electrochem. Sci. 8 (2013) 9459–9473.
[35] A.H. Reshak, Saleem Ayaz Khan, H. Kamarudin, Jiri Bila, J. Alloys Compd. 582 (2014) 6–11.
[36] L. Zhang, D.J. Singh, Phys. Rev. B 80 (2009) 075117.
[37] J.C. Li, C.L. Wang, M.X. Wang, H. Peng, R.Z. Zhang, M.L. Zhao, J. Liu, J.L. Zhang, L.M. Mei, J. Appl. Phys. 105 (2009) 043503.
[38] A. Popescu, L.M. Woods, J. Martin, G.S. Nolas, Phys. Rev. B 79 (2009) 205302.
[39] P. Blaha, K. Schwarz, J. Luitz, WIEN97, A Full Potential Linearized Augmented Plane Wave Package for Calculating Crystal Properties, Karlheinz Schwarz. Techn. Universit, Wien, Austria, 1991. ISBN:3-9501031-0-4.
[40] P. Hohenberg, W. Kohn, Phys. Rev. 136 (1996) B864.
[41] W. Kohn, L. Shom, J. Phys. Rev. 140 (1965) A1133.
[42] J.P. Perdew, A. Zunger, Self-interaction correction to density-functional approximations for many-electron systems, Phys. Rev. B 23 (1981) 5048.
[43] J.P. Perdew, K. Burke, M. Ernzerhof, Rev. Lett. 77 (1996) 3865.
[44] E. Engel, S.H. Vosko, Phys. Rev. B 50 (1994) 10498.
[45] F. Wooten, Optical Properties of Solids, Academic Press, New York, 1972.
[46] J. Ruiz-Fuertes, et al., Phys. Rev. B 86 (2012) 125202.
[47] R. Lacomba-Perales, et al., J. of Appl. Phys. 110 (2011) 043703.
[48] P. Debye, Dispersion of Roentgen rays, Ann. Phys. 46 (1915) 809.
[49] R.F.W. Bader, Atoms in Molecules – A Quantum Theory, Clanderon Press, Oxford, 1990.
[50] P. Coppens, Annu. Rev. Phys. Chem. 43 (1992) 663.
[51] D. Feil, J. Mol. Struct. 255 (1992) 221.
[52] F.L. Hirshfeld, in: A. Domenicano, I. Hargittai (Eds.), Accurate Molecular Structures. Their Determination and Importance, IUCr/Oxford University Press, Oxford, 1992, p. 237.
[53] F.L. Hirshfeld, Crystallogr. Rev. 2 (1991) 169.
[54] M.A. Spackman, Chem. Rev. 92 (1992) 1769.
[55] V.G. Tsirelson, R.P. Ozerov, J. Mol. Struct. 255 (1992) 335.
[56] G.A. Jeffrey, J.F. Piniella (Eds.), The Application of Charge Density Research to Chemistry and Drug Design, Plenum Press, New York, 1991.
[57] P. Coppens, X-ray Charge Densities and Chemical Bonding, Oxford University Press, Oxford, 1997.
[58] Studies of Electron distributions in Molecules and Crystals, in: R. Blessing (Ed.), Trans. Am. Crystallogr. Assoc. 26 (1990).
[59] W.J. Hehre, L. Radom, P.V.R. Schleyer, J.A. Pople, Ab Initio Molecular Orbital Theory, Wiley, New York, 1986.
[60] V. Quenéau, S.C. Sevov, Angew. Chem. 109 (1997) 1818. Angew. Chem. Int. Ed. Engl. 36 (1997) 1754.
[61] S. Lopez-Moreno, et al., Phys. Rev. B 84 (2011) 064108.
[62] N.M. Balzaretti, J.A.H. da Jornada, Solid State Commun. 99 (1996) 943.
[63] T.S. Moss, Proc. Phys. Soc. B 63 (1950) 167.
[64] V.P. Gupta, N.M. Ravindra, Phys. Stat. Sol. B 100 (1980) 715.
[65] A.L. Ruoff, Mater. Res. Soc. Symp. Proc. 22 (1984) 287.
[66] R.R. Reddy, S. Anjaneyulu, C.L.N. Samara, J. Phys. Chem. Solid 54 (1993) 635.
[67] P. Herve, L.K.J. Vandamme, Infrared Phys. Technol. 35 (1993) 609.
[68] N.M. Ravindra, S. Auluck, V.K. Srivastava, Phys. Stat. Sol. (B) 93 (1979). K155.
[69] L.E. Bell, Science 321 (2008) 1457.
[70] Francis J. Disalvo, Science 285 (1999) 703.
[71] G.J. Snyder, M. Christensen, E. Nishibori, T. Caillat, B.B. Iversen, Nat. Mater. 3 (2004) 458.